PERGAMON

International Journal of Heat and Mass Transfer 45 (2002) 2597–2609

International Journal of HEAT and MASS TRANSFER

www.elsevier.com/locate/ijhmt

Complete map out of the heat transfer coefficient at the surface of two circular cylinders $H/D = 3.0$ and 0.3 subjected to a cross-flow of air

Laetitia Ghisalberti, Alain Kondjoyan *

Equipe Génie des Procédés, Station de Recherches Sur la Viande, INRA, Theix, 63122 St Genès Champanelle, France

Received 20 October 2000; received in revised form 25 July 2001

Abstract

Transfer coefficients were mapped out using a constant heat flux method at the surface of two circular cylinders whose height to diameter ratios were 3.0 and 0.3, respectively. Cylinders were positioned cross to an air flow whose velocity was either near 1.0 m s^{-1} or near 4.0 m s^{-1} and turbulence intensity either 1.5% or 28%. The coefficient distributions both on the side and ends of cylinders are analysed in details. Variations of the mean transfer coefficients on the end and side of cylinders are studied separately to better understand the effect of H/D on the global transfer coefficient value.

1. Introduction

Many food processes, such as chilling, freezing, cooking and drying, are based on heat and water exchanges between a solid product and an air flow. To predict product temperature and weight loss, heat and mass transfer coefficients are used in models. Most often only the average value of transfer coefficient is considered although its value can be very different from one point of the product surface to the other. In some cases, the knowledge of the local transfer coefficient values can be of direct practical interest. For example to predict the risks of deterioration of the surface of the product during intense chilling or heating (very fast chilling, reheating or cooking). Moreover the knowledge of the distribution of the transfer coefficient is important to understand the variations of its average value.

Most studies on transfer coefficients reported in the literature describe the evolution of the coefficient value at the mid-height of a long (''infinite'') circular cylinder placed in a near laminar cross-flow of air. In practical conditions, however, although the shape of products is often cylindrical, they are short and are placed in highly turbulent flows. Studies have already been performed in the laboratory to study how flow turbulence and cylinder dimensions affect the average transfer coefficient value [1–3]. However very little is known on the effect of these factors on the distribution of the transfer coefficient. To our knowledge, the complete map out of the transfer coefficient has never been determined on a circular cylinder on the contrary to parallelepipeds and cubes [4,5].

The most detailed work on transfer coefficient distribution around a circular cylinder has been performed by Sparrow and Samie [6]. They have separated the mean mass transfer coefficient values measured on the top end from those measured on the side of long cylinders attached by their bottom end to the experimental cell. However during this study only a few coefficient distributions were really measured on the side of the cylinder and the distribution on the top end was not examined.

The distribution of transfer coefficient depends on the flow which develops at the body surface (boundary layer flow). The structure of this boundary layer on the free end and side of a short circular cylinder is not really known. To our knowledge, no work has been done on the effect of two free ends on the structure of the boundary flow around the side of the cylinder.

* Corresponding author. Tel.: +33-4-7362-4492; fax: +33-4-7362-4089.

E-mail address: alain.kondjoyan@clermont.inra.fr (A. Kondjoyan).

0017-9310/02/$ - see front matter
PII: S0017-9310(01)00352-0

Nomenclature

Latin symbols

D	cylinder diameter (m)
H	cylinder height (m)
h	heat transfer coefficient (W m^{-2} K^{-1})
T_s	temperature at the surface of the cylinder (°C or K)
T_{air}	air temperature (°C or K)
Tu	turbulence intensity in the main flow direction : $\sqrt{\overline{u^2}}/U$ (%)
Nu	Nusselt number $= h \cdot D/\lambda_a$
u	velocity fluctuation around U (m s^{-1})
U	mean air velocity in the flow direction (m s^{-1})
y	distance from the top end of the cylinder in the cross-flow direction (m)

Greek symbols

ε	emissivity of the cylinder surface
Φ	heat flux at the wall (W m^{-2})
θ	angle from the stagnation point of the cylinder (degree)
λ	thermal conductivity of the wire (W m^{-1} K^{-1})
λ_a	thermal conductivity of the air (W m^{-1} K^{-1})
σ	Stefan–Boltzmann constant (W m^{-2} K^{-4})

Mean

$\bar{x}$	mean of x

Studies have been performed in water to determine the effect of cylinder ends on wake flow. During these experiments the bottom of the cylinder was attached to the floor of a tank and the top of the cylinder was above the water surface [7]. The end effects were due both to the presence of the water surface and to the bottom end of the cylinder. It is difficult to use these results in the present case since in this study Reynolds numbers were very small and phenomena which developed at the water surface were preponderant.

A recent study was performed by Tanaka and Murata [8] in air on cylinders with an aspect ratio in between 1.25 and 10 which were attached by their bottom end ($Re = 3.7 \times 10^4$). During their detailed analysis of the structure of the side wake, Tanaka and Murata observed that the effect of the longitudinal vortices which might be shed from the top end of the cylinder was hardly perceptible. However the presence of this free end induced three dimensional effects in the wake by bowing the vortex lines which joined the lateral vortices.

Momentum transfers are also governed by the boundary flow. The effect of a free end on the distribution of the pressure coefficients on the side of a circular cylinder has been studied by Farivar [9] for Reynolds numbers in between 2×10^4 and 7×10^4. Similar studies have also been reviewed by Basu [10]. Results show that the presence of one free end modifies the distribution of the pressure coefficient on the side of the cylinder even for aspect ratio as great as 15. The presence of the free end leads to a smaller coefficient value at its nearby which tends to increase toward the bottom and then stabilises. Variations are most often greater in the wake than upstream separation. According to Farivar [9], the structure of the wake is tridimensional near the top end while it is mainly two-dimensional in the middle of the cylinder.

Flow movement was also visualised by Sparrow and Samie [6] on the top end and side of attached cylinders. They covered the cylinders with an oil–lampblack mixture which moves under the action of the shear stresses due to the air flow. The resulting flow patterns will be discussed with the results of the present paper.

In this study, a method developed recently at the laboratory [11] was used to map out the local heat transfer coefficient all over the surface of two circular cylinders whose aspect ratios were $H/D = 0.3$ and 3.0, respectively. The shape of many food products is close to the shape of a cylinder which aspect ratio ranges from 0.3 to 3.0. Moreover one of the objectives of this study was to analyse average results obtained previously on cylinders in the same range of H/D.

Cylinders were not directly attached to the floor of the experimental cell but supported using a rod (two free ends). They were subjected to a cross-flow of air whose velocity was either near 1.0 m s^{-1} or near 4.0 m s^{-1} and whose turbulence intensity was either 1.5% or 28%. Results obtained under a turbulence intensity of 1.5% can be compared to the results of literature. A turbulence intensity of 28% corresponds to the level of velocity fluctuations measured during a previous study inside a food products dryer [12]. To improve the analysis of the results, the flow on the top end of the cylinder $H/D = 3.0$ was visualised using the same technique as Sparrow and Samie [6].

2. Materials and methods

2.1. Measurement of the heat transfer coefficients

The heat transfer coefficient was determined using a constant heat flux method combined with a measurement of surface temperatures by an infrared camera (type TVS 2100 MKII of Nippon Avionics Corporation). More details on the technique, picture processing,

assessment of bias and errors can be found in previous publications [11].

Heat transfer coefficients had to be determined all over the cylinder surface, that is on its side as well as on its ends. In this case, the classic heating ribbon technique cannot be used to cover both the side and ends of the object. Thus the ribbon was replaced by an oxy-insulated electrical wire made in Nickel–Chrome (60% Nickel and 15% Chrome $\lambda = 13$ W m^{-1} K^{-1}, wire diameter 0.8 mm) which can be continuously coiled to cover the surface of cylinders.

Cylinders were hollow (0.108 m in diameter), made in polypropylene (0.8×10^{-3} m in thickness) and filled with glass wool. The cylinder $H/D = 3.0$ was not totally coiled with the wire to lighten the technical work and to respect the limits of the electrical generators. The coiled area corresponded to all the top end and the 0.20 m of the side of the cylinder adjacent to this end. To limit the exchanges by conduction between the coiled and non-coiled area, these two parts were separated by a 0.02 m wide guard heater which had its own electrical supply.

The main technical difficulty was continuously coiling the wire on the end and connecting this part to the wire loops located on the side of the cylinder. When the wire was coiled, the cylinder was covered with mastic to smooth its surface and black paint to have an infrared emissivity as close to one as possible.

In the last stage 1 mm wide aluminium strips were stuck at regular intervals along the perimeter and height of the cylinder side. These strips had a low emissivity and were used as markers during the treatment of infrared pictures. Seven strips were positioned on the perimeter of the cylinder $H/D = 3.0$ and twenty two along its height.

The cylinder $H/D = 0.3$ was built with the same material and following the same techniques as for the cylinder $H/D = 3.0$. Its surface was completely coiled (side + 2 ends) with the wire except in the area where there was the rod which supported the sample. Seven aluminium strips were positioned on its perimeter and two along its height.

A schematic representation of the experimental apparatus is shown in Fig. 1. During the experiments, the sample was located inside the experimental cell (0.8 m × 0.8 m × 1.60 m) of a wind tunnel which has already been described elsewhere [1,2]. Cylinders were positioned either horizontally or vertically depending whether the infrared pictures had to be taken on the ends or side. Air temperature in the wind tunnel was close to 25 °C and was precisely measured near the sample using a PT100 probe. The residual free stream turbulence intensity inside the wind tunnel was near 1% and could be increased up to 28.0% by placing perforated plates in drawers located upstream from the experimental cell [1,2]. Before heat coefficients measurement, air velocity and turbulence intensity were measured accurately at the location where the sample was to be placed using a hot wire anemometer.

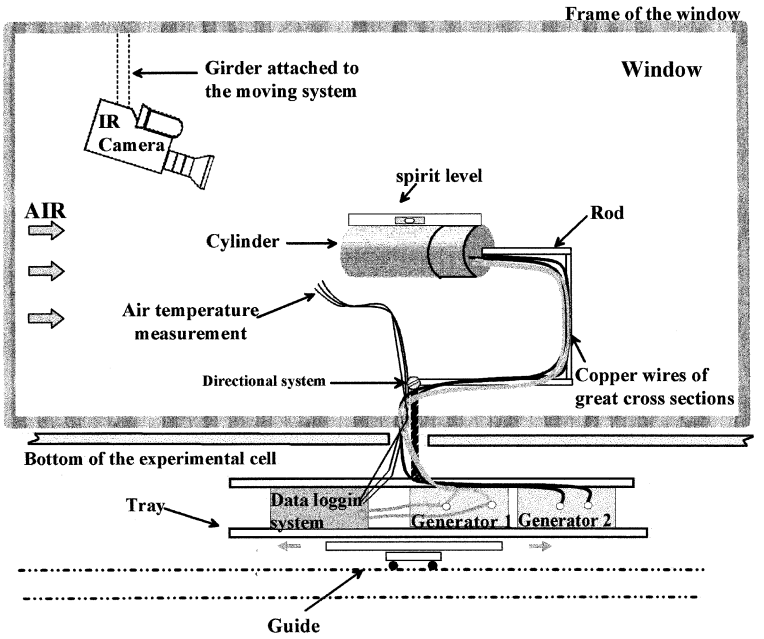

Fig. 1. Schematic representation of the apparatus used in the experimental chamber of the wind tunnel to map out the heat transfer coefficient at the surface of the circular cylinders. The sample is represented here in a horizontal position which was used to make the infrared pictures on ends.

To avoid undesirable flow disturbances, the infrared camera was located outside the experimental cell (Fig. 1). Thus, surface temperatures had to be measured through a window which occupied one of the cell walls. The window was made of a 10^{-3} m thick polyethylene film which had proved to be almost fully transparent to infrared radiation. Moreover to measure surface temperatures accurately the response of the infrared camera was calibrated in situ using a flat target built especially for that purpose [11].

When a constant heat flux is generated at a solid surface and when the steady-state period is reached, the heat transfer coefficient h can be directly determined from the energy balance by:

$$h = \underbrace{\frac{\Phi}{T_s - T_{air}}}_{(I)} - \varepsilon\sigma \underbrace{\frac{T_s^4 - T_{air}^4}{T_s - T_{air}}}_{(II)}. \quad (1)$$

Term (I) describes the transfer by convection and (II) the transfer by radiation. T_s and T_{air} are the surface and air temperature (expressed in Kelvin), respectively. ε is the emissivity of the solid σ the Stefan–Boltzmann constant.

During the experiments, the cylinder surface was heated to a temperature between 50 and 60 °C. When the infrared camera had been carefully calibrated, it was possible to measure the surface temperature with an error less than +/− 0.5 °C. The accuracy of the other measurements ensured that the overall error in determining the heat transfer coefficient was always less than 5% of the given result [11].

Each surface temperature picture from the infrared camera system led to a matrix of data whose size was 100×256 pixels (video format). On the top end of the cylinders, one picture was enough to see all the surface. To obtain the complete coefficient distribution on half the perimeter of the cylinder side (transfers were symmetrical on the other half of the perimeter), a combination of four pictures was necessary. As pictures of temperature were geometrically distorted and not exactly the same in size and position, they had to be treated before being combined. Thus picture processing programs were developed using the Matlab software (version 5.2 completed by its image processing toolbox).

During picture processing, one of the main difficulties was to describe the areas located just near the cylinder edges where the transfers were very intensive (surface temperature on the object close to the temperature of the background). This concerned the top and bottom of the cylinder side and the area close to the rim of the cylinder end. Here the exact location of the frontier between the cylinder and the background was difficult and the error on the transfer coefficient value was greater. Preliminary trials had shown that the problem was limited to the three to five first millimetres near the edges of the cylinder. Thus the following images on the end of the cylinders correspond to the picture of the surface minus the three first millimetres located against the rim. On the side of the cylinder $H/D = 3.0$, the top and bottom first five millimetres which add nothing to the discussion of results have also been eliminated. In the case of the side of the cylinder $H/D = 0.3$, the surface was very short. The whole image was kept even if the exact location of the top and bottom edges and the exact value of the transfer coefficients on the borders could be a little erroneous.

2.2. Visualisation of the flow at the surface of the cylinders

Flows at the surface of the cylinders were visualised using the same technique as Sparrow and Samie [6]. In this technique, a mixture of oil and powder is brushed on the body surface. The powder colours the oil and modifies its density. Under the action of the shear stresses due to the flow, the mixture moves along the surface following the fluid paths. Regions of high velocities appear as uncoloured streaks while regions of low velocities where the mixture is stationary remain coloured and streak-free.

During our experiments, the lampblack powder used by Sparrow and Samie was replaced by a coloured chalk powder commonly used for line-tracing by masons and electricians. Different kinds of oils of different viscosity were tested.

As Sparrow and Samie pointed out, very stiff mixtures are needed on the side of cylinders to avoid these mixtures flowing down by gravity. Sparrow and Samie were able to move such stiff mixtures using air velocities greater than 20 m s^{-1}. During our experiments, air velocities were less than 5.0 m s^{-1} and the stiff mixtures could not move. Hence no visualisation was possible on the side of cylinders.

On the top end of cylinders flowing by gravity was not a problem. Very fluid mixtures could be used to follow air movement. Types of oil which could be mixed with water were chosen. The right density of the mixture was obtained by adding chalk powder and the right fluidity by adding water to the oil. Photographs of the flow patterns obtained on the top end of the cylinder $H/D = 3.0$ for air velocities of 1.0 and 4.0 m s^{-1} are given bellow. As these photographs cannot fully render the fluid movement, they are accompanied by schematic representations of what was observed.

3. Results

Results are presented in two stages. In the first stage the evolution of the heat transfer coefficient distribution with the main flow properties is described. Coef-

ficients are divided by their mean value ($h/\overline{h} = Nu/\overline{Nu}$) calculated on the concerned area (either end or side). This representation is not the classical one but it enables the comparison of map outs obtained under different air velocity and turbulence intensity conditions. When possible, transfer coefficient map outs are discussed in the light of flow patterns. In the second stage, the mean variations of the transfer coefficients on the end and side of cylinders are studied separately to better understand the effect of H/D on the global transfer coefficient value.

3.1. Coefficient distributions on the side of cylinders

3.1.1. Side of cylinder $H/D = 3.0$

The four coefficient map outs obtained under the different main flow conditions on the cylinder side are shown in Fig. 2. Some heat transfer coefficient profiles determined in the flow direction at different distances from the top end of the cylinder are shown in Fig. 3.

Whatever the proximity to the top end of the cylinder (as close as 10^{-2} m from this end), profiles keep globally the well-known feature of the 2 Dimensions profile

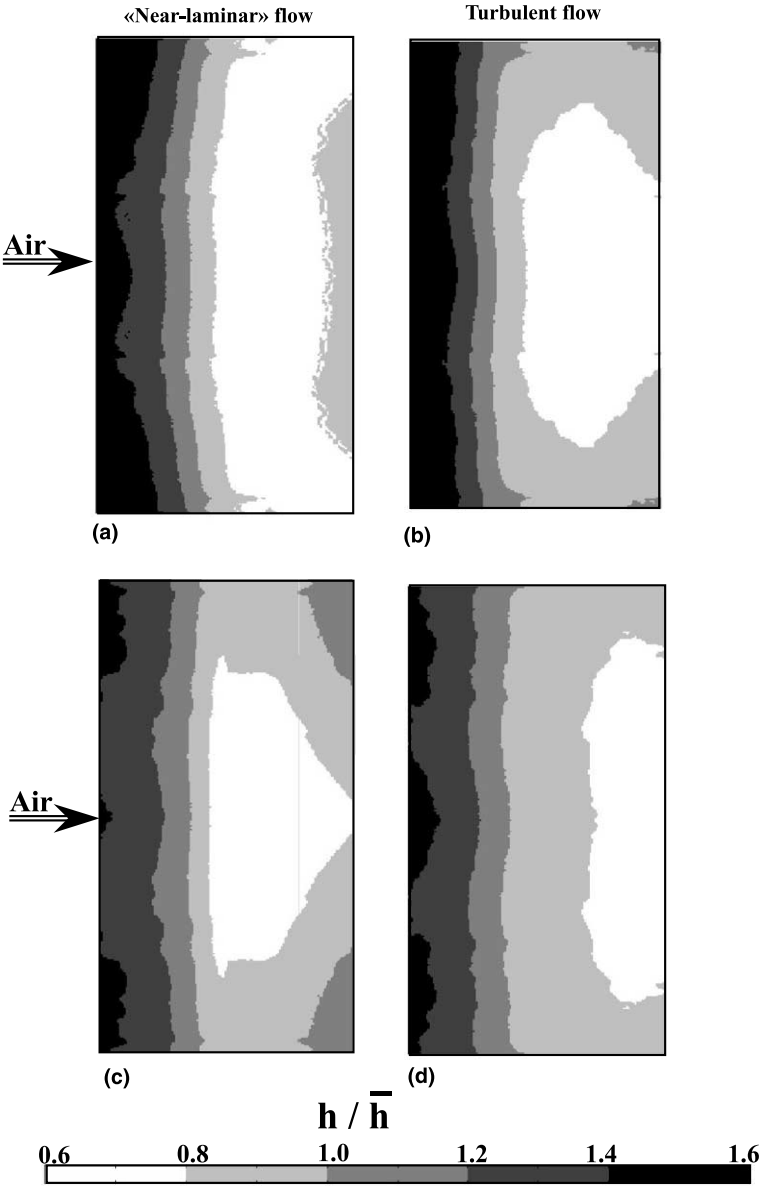

Fig. 2. Map out of the transfer coefficient on the side of the cylinder $H/D = 3.0$ obtained under the following conditions: (a) $U = 0.77$ m s^{-1}, Tu = 1.5%; (b) $U = 1.4$ m s^{-1}, Tu = 28.0%; (c) $U = 3.85$ m s^{-1}, Tu = 1.5%; (d) $U = 4.45$ m s^{-1}, Tu = 28.0%.

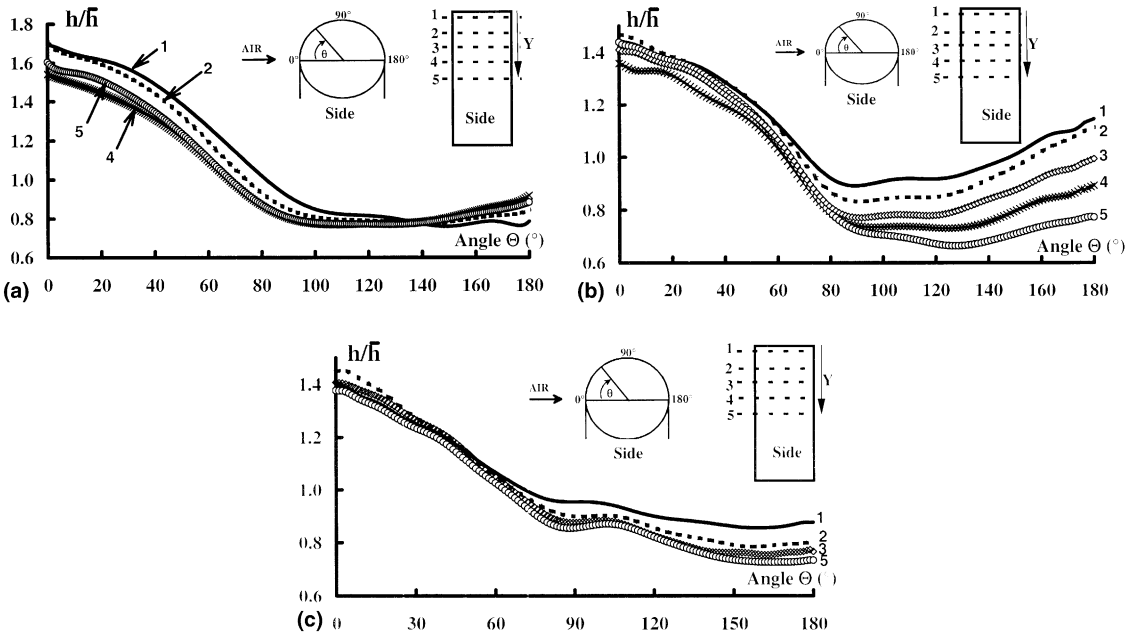

Fig. 3. Heat transfer coefficient profiles determined in the free steam direction at different distances from the top end of the cylinder $H/D = 3.0$: (1) $y = 1 \times 10^{-2}$ m; (2) $y = 4 \times 10^{-2}$ m; (3) $y = 8 \times 10^{-2}$ m; (4) $y = 12 \times 10^{-2}$ m; (5) $y = 16 \times 10^{-2}$ m. Main flow conditions were: (a) $U = 0.77$ m s^{-1}, Tu = 1.5%; (b) $U = 3.85$ m s^{-1}, Tu = 1.5%; (c) $U = 4.45$ m s^{-1}, Tu = 28.0%.

existing on the "infinite cylinder". The coefficient decreases from the stagnation to the separation point and then follows more complex variations in the wake (Fig. 3). However despite this overall unity, profiles differ in some details according to the distance from the top end.

In the stagnation area when Tu = 1.5%, the heat transfer coefficient value decreases in the cross-flow direction from the vicinity of the end (No. 1, Figs. 3(a) and (b)) toward a minimum (reached at level No. 4, Figs. 3(a) and (b)) and then increases to a maximum value at the mid-height of the cylinder (No. 5, Figs. 3(a) and (b)). This up-down distribution in the maps out gives the lines of equal transfer coefficient values located near the stagnation area a bracket shape, i.e. (Fig. 2).

In the wake, distributions vary according to the main flow conditions.

When $U = 0.77$ m s^{-1}, Tu = 1.5%, the heat transfer coefficient value which is small near the cylinder end increases to reach a maximum at height-level No. 4, (Fig. 3(a)).When $U = 3.8$ m s^{-1}, Tu = 1.5%, differences are very large in the wake and the heat transfer coefficient decreases regularly with the distance from the ends (Fig. 3(b), decrease from (1) to (5)).

When the free stream turbulence intensity is 28%, differences between the profiles become very small. For $U = 1.4$ m s^{-1}, Tu = 28%, differences are hardly visible and not shown here. For $U = 4.45$ m s^{-1}, Tu = 28%, profiles present an unusual and original feature (Fig. 3(c)). A second maximum tends to occur after separation (preceding sign of a laminar-turbulent transition?) followed downstream by a decrease in the heat transfer coefficient. This decrease in the downstream wake is clearly visible in the map out where it appears as a large white dead zone (Figs. 2(b) and (d)).

As we were not able to visualise the flow on the side of the cylinders, a full interpretation of the coefficient distributions is difficult and remains under discussion. However it is possible to suggest some explanations based on the results in the literature.

The fact that on the top and bottom edges (not represented in Fig. 2) and in the upstream corners of the cylinder surface transfers are greater has already been observed on cubes [5]. This result is commonly explained by the turbulence generated in the flow by edges and corners.

Present results have shown that the profiles on the side of the cylinder always resemble the well-known 2D profile. This can be explained by the observations of Tanaka and Murata [8] on the small effect of the longitudinal vortices shed from the end of the cylinder on the structure of the wake. The fact that the effect of the free ends tends to be greater in the wake when the flow velocity is high (Fig. 3(b)) is in accordance with the results of Farivar and Basu [9,10]. Moreover extension of the white dead zone existing in the wake with the free stream turbulence intensity (Figs. 2(b) and (d)) can reasonably be explained by a disorganisation of the formation of vortices due to external turbulence (external turbulence is known to inhibit the development of separation–reattachment vortices).

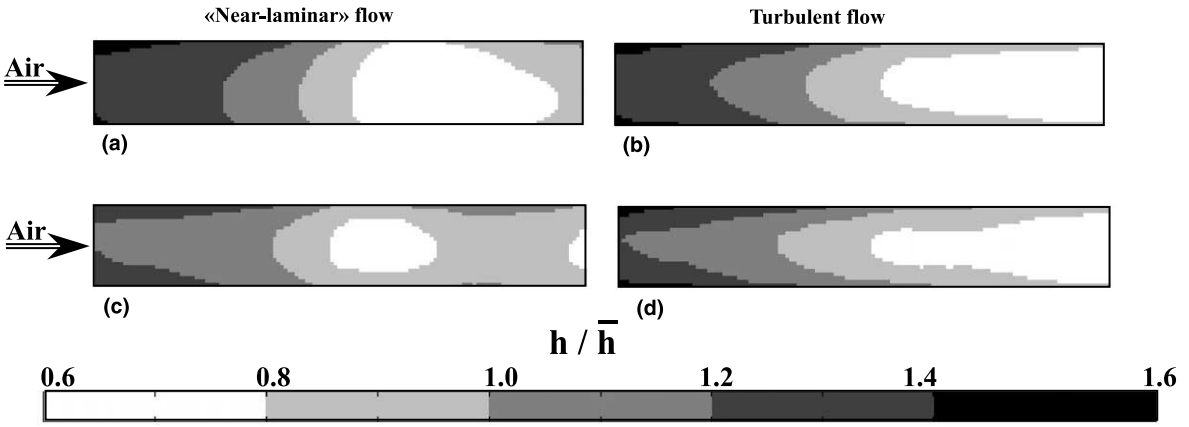

Fig. 4. Map out of the heat transfer coefficient on the side of the cylinder $H/D = 0.3$ obtained under the following conditions: (a) $U = 0.77$ m s^{-1}, Tu = 1.5%; (b) $U = 1.4$ m s^{-1}, Tu = 28.0%; (c) $U = 3.85$ m s^{-1}, Tu = 1.5%; (d) $U = 4.45$ m s^{-1}, Tu = 28.0%.

3.1.2. Side of cylinder $H/D = 0.3$

The four coefficient map outs obtained under the different main flow conditions on the side of the cylinder $H/D = 0.3$ are shown in Fig. 4. Coefficient profiles obtained in the flow direction under three of the four previous conditions at mid-height of the cylinder are presented in Fig. 5.

On the side of the cylinder $H/D = 0.3$, in spite of the very close vicinity of the ends profiles overall maintain the feature which exists on an infinite cylinder (Fig. 5). However the separation point moves downstream (θ equal to about 120°).

On the map outs, when Tu = 1.5%, $U = 0.77$ m s^{-1} the greater transfers existing on the upstream corners and edges are clearly visible (Fig. 4(a)). This "corner effect" leads to a round shape of the lines of equal coefficient value. In the wake, these lines are distributed concentrically. The transfer coefficient value which present a single minimum at about $\theta = 120°$ increases downstream in the wake (No. 1, Fig. 5).

When Tu = 1.5%, $U = 3.8$ m s^{-1}, there are two zones in the wake where the heat transfer coefficients are very low (Fig. 4(c), No. 2 in Fig. 5). The width of the peak which separates these two zones is large and does not have the usual appearance of a peak of laminar-turbulent transition (No. 2, Fig. 5).

When the free stream turbulence increases, there is comparatively less transfer intensification due to upstream corners and lines of equal coefficient value become "elliptic" (Figs. 4(b) and (d)). As before for the cylinder $H/D = 3.0$, the heat transfer coefficient value decreases after separation in the wake (No. 3, Fig. 5).

One can observe that some features of the coefficient distributions are common on the cylinder $H/D = 0.3$ and on the cylinder $H/D = 3.0$. Except for the suggestions proposed previously to explain these common features, it seems hazardous to go further in the analysis because of the complete lack of knowledge about the flow pattern which exists on the side of the cylinder $H/D = 0.3$.

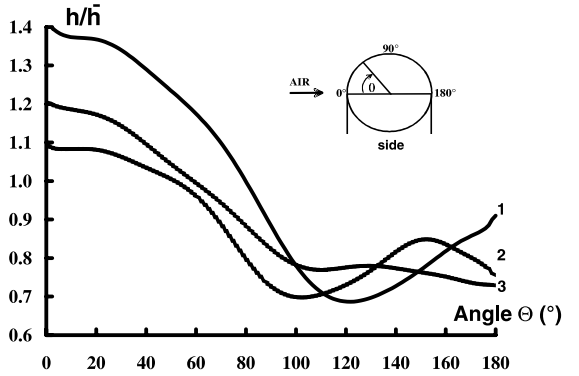

Fig. 5. Heat transfer coefficient profiles in the free steam direction at mid-height of the cylinder $H/D = 0.3$ obtained under the following conditions: (1) $U = 0.77$ m s^{-1}, Tu = 1.5%; (2) $U = 3.85$ m s^{-1}, Tu = 1.5%; (3) $U = 4.45$ m s^{-1}, Tu = 28.0%.

3.2. Coefficient distributions on the ends of the two cylinders

3.2.1. Description of the coefficient distributions

Circular map outs obtained on the ends of the two cylinders are shown in Figs. 6 and 7. Heat transfer coefficient profiles measured on the line parallel to the flow direction and which crosses the middle of the circles are given in Fig. 8.

When $U = 0.77$ m s^{-1}, Tu = 1.5%, the heat transfer coefficient value which is great on the upstream rim (upstream edge of the circle) decreases sharply downstream to a minimum and then increases again (Figs. 6(a) and (b) and 8). The lines of equal coefficient value

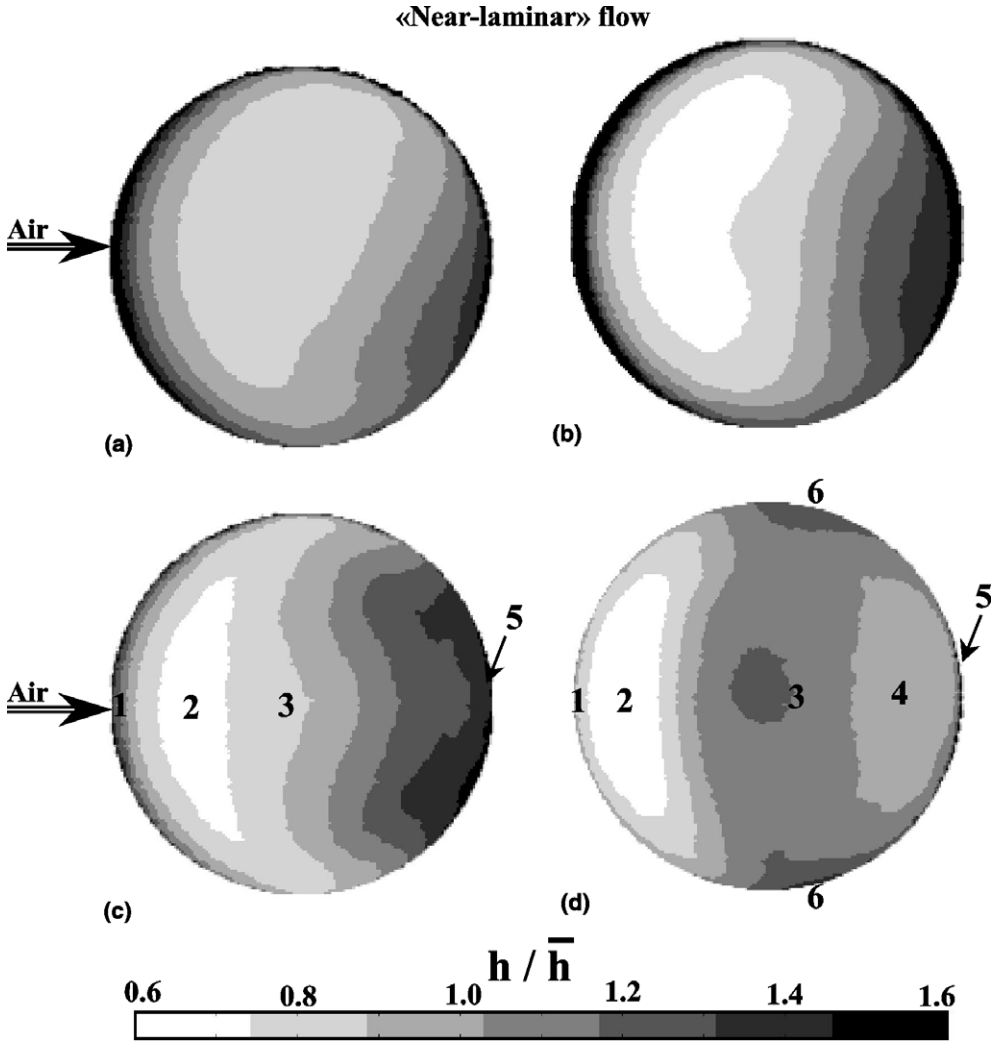

Fig. 6. Map out of the heat transfer coefficient on the ends of the cylinders $H/D = 3.0$ (left) and $H/D = 0.3$ (right) when the turbulent free stream intensity was 1.5%. On the top of the figure (a, b) $U = 0.77$ m s^{-1}, on the bottom (c, d) $U = 3.85$ m s^{-1}.

take on a crescent shape which is more pronounced for the cylinder $H/D = 0.3$ than for the cylinder $H/D = 3.0$ (Figs. 6(a) and (b)). The slight asymmetry which exists between the top and the bottom of the map out is due to free convection.

When U is around 4.0 m s^{-1} and Tu = 1.5%, the extension of the crescent-shaped area where transfers are minimum decreases (Figs. 6(c) and (d)). Distribution is different on the cylinder $H/D = 3.0$ compared to the cylinder $H/D = 0.3$.

On the cylinder $H/D = 3.0$ (Figs. 6(c) and 8(a)), the heat transfer coefficient increases regularly from the crescent-shaped area further downstream (from (2) to (5)). Downstream from the crescent shape area (2) is an area (3) where the lines of equal coefficient value have curious "bracket-shaped" features (Fig. 6(c)). The area located completely up against the downstream rim (5) also has a very specific shape.

On the cylinder $H/D = 0.3$ (Figs. 6(d) and 8(b)), the heat transfer coefficient increases from the crescent-shaped area (2) to a maximum located in (3) then decreases in (4) and increases again against the downstream rim (5). There are no braked-shaped features of the lines of equal coefficient value in the area (3). However two small spot areas (6) exist at the top and bottom of the coefficient distribution (Fig. 6(d)).

When the free stream turbulence increases, map outs are completely destructured whatever the air velocity (Fig. 7). On the cylinder $H/D = 3.0$, the heat transfer coefficient value is perfectly constant except on the rim where it is higher (Figs. 7 and 8(a)). For $H/D = 0.3$, the situation is similar except that the heat transfer coeffi-

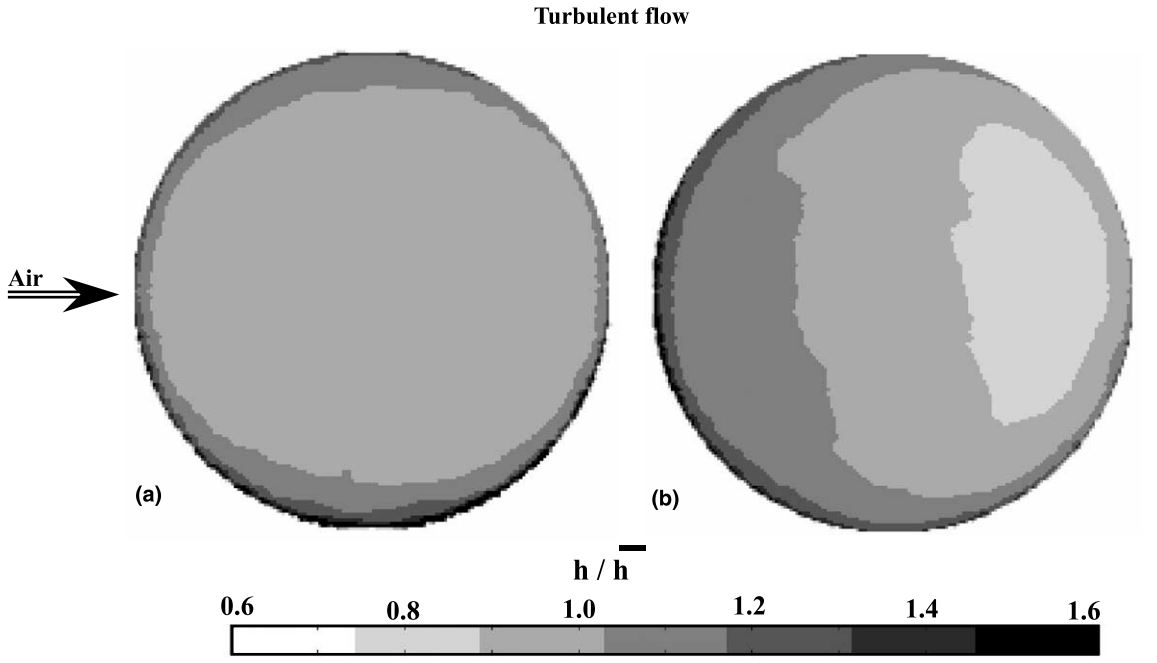

Fig. 7. Map out of the heat transfer coefficient on the ends of the cylinder (a) $H/D = 3.0$, (b) $H/D = 0.3$ when the turbulent free stream intensity was 28% and the main flow velocity 4.45 m s^{-1}.

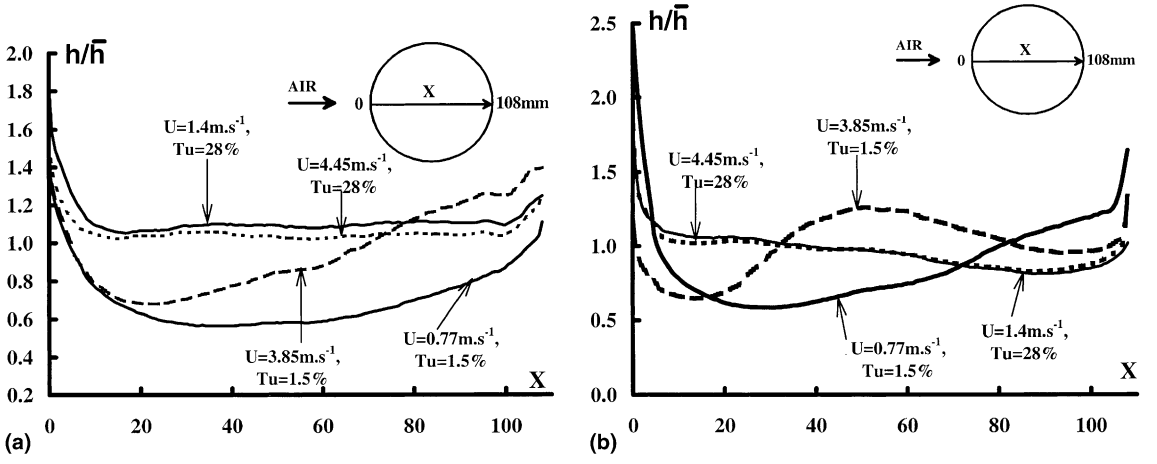

Fig. 8. Heat transfer coefficient profiles measured under different main flow conditions on the end of the cylinder (a) $H/D = 3.0$, (b) $H/D = 0.3$ in the line parallel to the flow direction and which crosses the middle of the circle.

cient value is slightly higher in the upstream part of the cylinder end than on its downstream part (Figs. 7(b) and 8(b)).

3.2.2. Analysis of the map outs in the light of flow patterns

Only the map outs obtained when Tu = 1.5% are analysed in the following since no clear flow pattern could be determined when Tu = 28%.

The flow pattern as seen by Sparrow and Samie [6] is schematised by us in Fig. 9. According to their description, six different areas can distinguished. Against the upstream rim the flow separates (I) going up over the cylinder surface. Immediately downstream of the rim stands a vast crescent shaped area where the boundary velocity is very low (II). Further downstream stands another area (IV) of very low velocity which is also

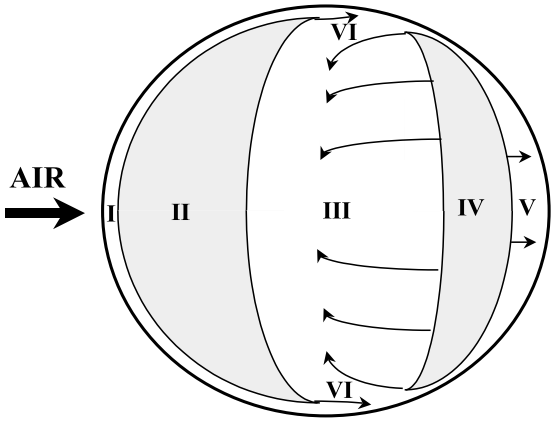

Fig. 9. Schematic representation of the flow based on the experiments of Sparrow and Samie [6].

shaped like a crescent but is oriented in the opposite direction to (II). According to Sparrow and Samie the flow becomes reattached at the surface just at the upstream border of this crescent area (II). Between area (II) and (IV) stands a recirculating zone (III) where the air velocity is opposite to the main flow direction. Near the flank of the crescent-shaped area (IV) and downstream, there are two zones (V) and (VI) where the velocity is oriented in the main flow direction.

The six regions (1)–(6) of the coefficient map out obtained on the cylinder $H/D = 0.3$ for $U = 3.8$ m s^{-1} (Fig. 6(d)) match perfectly the areas (I)–(VI) of the flow pattern described by Sparrow and Samie. However it does not explain why the crescent shape area (4) does not exist on the other map outs (Figs. 6(a), (b) and (d)). Neither does it explain why for $U = 4.45$ m s^{-1}, Tu = 1.5% the lines of equal coefficient value exhibit curious bracket-shape features in the area (3) for the cylinder $H/D = 3.0$ (Fig. 6(c)). These contradictions have led us to visualise the flow pattern on the top end of the cylinder $H/D = 3.0$.

The resulting visualisations obtained for $U = 1.0$ and 4.45 m s^{-1} are shown in Figs. 10(a) and (b), respectively. Photographs are accompanied by diagrams that describe the structure of the flow.

When the air velocity is 1.0 m s^{-1} (Fig. 10(a)), after the flow separates on the upstream rim there exists an

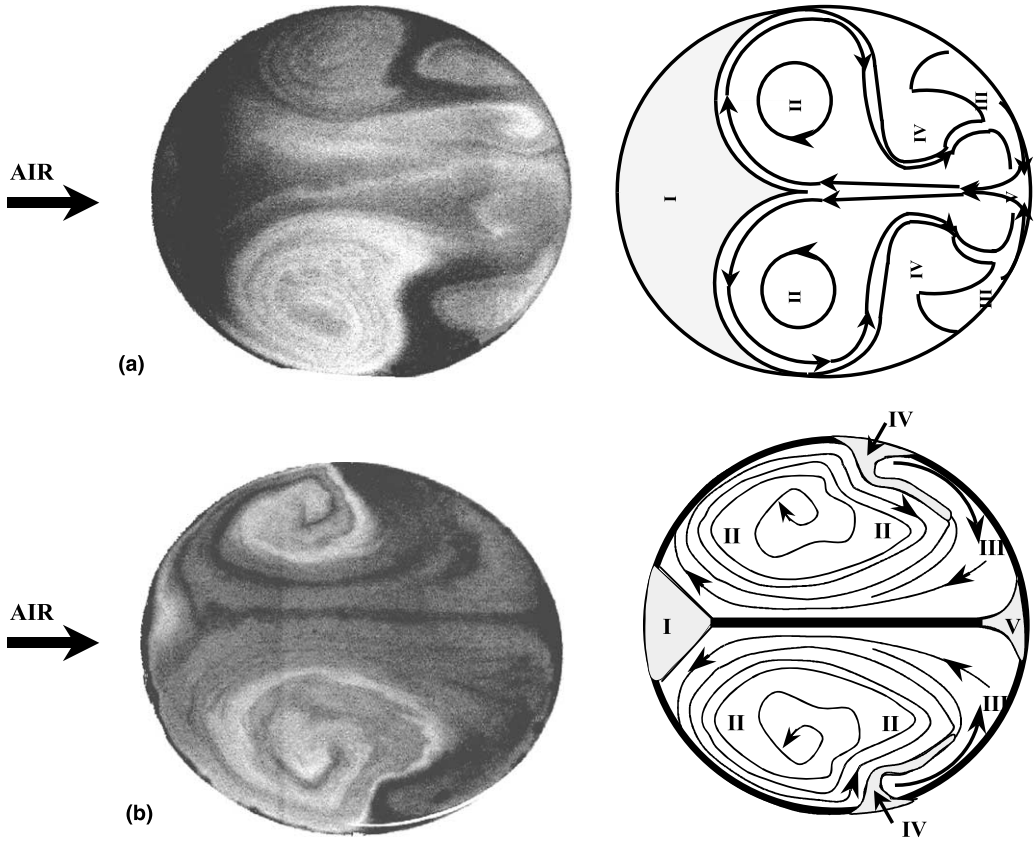

Fig. 10. Flow visualisation obtained during the present study for Tu = 1.5% on the top end of the cylinder $H/D = 3.0$: (a) $U = 1.0$ m s^{-1}; (b) $U = 4.45$ m s^{-1}.

area (I) where the boundary velocities are very low. Flow reattachment occurs against the downstream rim (III) symmetrically and in a circular way from the outside to the inside of the disk. In between, it leaves an area (V) where the boundary velocities are smaller. The reattached flow goes in the opposite direction to the main flow leading to the formation of two contra-rotating vortices (II) which are symmetrical with respect to the middle line which crosses the centre of the disk. The two vortices (II) are not circular but become elongated into two little lobes taking the shape of human ears which join area (III). Between the two little lobes and the rim is an area (IV) where the boundary velocity seems to be smaller.

When the air velocity increases (Fig. 10(b)), the two vortices (II) spread leading upstream to an almost disappearance of area (I) which remains only through a "v shape region". The reattachment area (III) also spreads upstream following the rim while areas (IV) and (V) shrink.

The previous flow pattern enables a better comprehension of some features of the coefficient map outs which were difficult to explain following the results of Sparrrow and Samie [6]. For example because the flow reattachment (III) is located against the downstream rim (Fig. 10), it is logical that no crescent area (4) appears on the map outs of Figs. 6(a)–(c). Moreover the two vortices (II) existing in the flow explain the curious bracket-shape of the lines of equal coefficient value which can be observed in Fig. 6(c). One has just to draw lines which are supported by the contours of the two vortices (II) to obtain this shape (such a line forms the frontier between Region (I) and (II) in Fig. 10(a)). However a lot of details which can be observed in the flow do not appear in the map outs. For example areas (I), (IV), (V) which can be observed in Fig. 10 cannot be distinguished from other regions in Figs. 6(a)–(c).

3.3. Evolution of the average heat transfer coefficient value with H/D

It is possible using the previous map outs to analyse separately the evolution of the heat transfer coefficient on the end and on the side of the two cylinders. The global average value of the heat transfer coefficient can be re-calculated from the values obtained on the side and ends by

Table 1
Side and ends surfaces divided by the total surface and expressed in percentage for the two cylinders $H/D = 3.0$ and 0.3

H/D	$1/(1+F)$	$F/(1+F)$
3.0	85	15
0.3	37	63

Table 2
Heat transfer coefficient values on the side, ends and totality of the cylinder surface

Flow		Side			Ends			Global		
U (m s^{-1})	Tu (%)	H/D		Ratio (II)/(I)	H/D		Ratio (IV)/(III)	H/D		Ratio (VI)/(V)
		$3.0^{(I)}$	$0.3^{(II)}$		$3.0^{(III)}$	$0.3^{(IV)}$		$3.0^{(V)}$	$0.3^{(VI)}$	
0.77	1.5	10.4	11.3	1.09	7.1	8.2	1.16	9.9	9.4	0.94[a]
3.85	1.5	27.6	34.2	1.24	26.8	37.7	1.41[b]	27.4	36.4	1.33[b]
1.40	28	17.5	21.8	1.24	20.8	20.5	0.99	18.0	21.0	1.17
4.45	28	40.0	47.0	1.18	46.5	45.3	0.98	40.9	46.0	1.12

Ratios of the coefficients obtained on the cylinder $H/D = 0.3$ to those obtained on the cylinder $H/D = 3.0$.
[a] Paradox due to the respective part of the side and ends surfaces.
[b] Greatest effects of H/D.

$$\overline{h} = \frac{h_{\text{side}} + F \cdot h_{\text{end}}}{1 + F}, \quad (2)$$

where F is a shape parameter equal to $1/2\left(\frac{H}{D}\right)^{-1}$ in the case of a circular cylinder.

Ratios $1/(1+F)$ and $F/(1+F)$ represent the fraction of the side surface and the end surface divided by the total cylinder surface, respectively. These ratios calculated for the two cylinders $H/D = 3.0$ and 0.3 are given in Table 1. Even for the very short cylinder $H/D = 0.3$ the part of the side surface, which is involved in the heat transfer, represents near 40% of the total cylinder surface.

Table 2 gives the mean heat transfer coefficient values calculated under the different main flow conditions. Evolution of the heat global transfer coefficient agrees completely with previous results obtained from another experimental method [3]. The global heat transfer coefficient value on the cylinder $H/D = 0.3$ is always significantly greater (except when $U = 0.77$ m s^{-1}, Tu = 1.5% where there is a 6% decrease in $\overline{h}$) than the value measured on the cylinder $H/D = 3.0$. The greatest difference between the two cylinders is observed when Tu = 1.5% and U is around 4.0 m s^{-1}.

Table 2 shows how the mean values obtained on the side and ends of the cylinder leads to the global effect of H/D.

When the free stream turbulence equals 28%, the effect of H/D comes from a heat transfer coefficient value on the side of the cylinder which is greater for $H/D = 0.3$ than for $H/D = 3.0$. This is probably due to the great turbulence generated by the ends of the cylinders $H/D = 0.3$ on its side.

When $U = 3.8$ m s^{-1}, Tu = 1.5%, the global effect of H/D comes from the heat transfer coefficient value on the end of the cylinder $H/D = 0.3$ which is much greater than on the end of cylinder $H/D = 3.0$.

The condition $U = 0.77$ m s^{-1}, Tu = 1.5% leads to a paradox. The decrease in H/D leads to a greater mean transfer coefficient value both on the ends and side of the cylinder. Despite this the global transfer coefficient value decreases a little. This is because the fraction of the transfer coefficient on the side of the cylinder – which is always greater than on its ends- decreases with H/D (as $1/(1+F)$ decreases see Table 1).

4. Conclusions

The detailed analysis of the heat transfer coefficient map outs obtained on the two cylinders $H/D = 3.0$ and 0.3 leads to the following conclusions:

- on the side of the two cylinders whatever the vicinity of their ends the coefficient profiles in the free steam direction keep generally the 2D classical features encountered at the surface of an infinite cylinder;
- transfer coefficients are always greater on the upstream corner of the cylinders side than everywhere else at the cylinder surface;
- when the free-stream turbulence is low, map outs on the ends of the cylinders show original features which can be explained by the flow patterns; these original features disappear when free stream turbulence increases.

The separate observations of variations in the mean heat transfer coefficient measured on the ends and side of the cylinders leads to a better comprehension of the global effect of H/D. However, more research is needed on flow patterns especially on the side of circular cylinders to better understand heat transfer coefficient map outs.

Acknowledgements

The authors thank A. Lasteyras, J.M. Auberger and F. Peyrin for their technical collaboration and C. Young for revising the English manuscript.

References

[1] A. Kondjoyan, J.D. Daudin, Effects of free stream turbulence intensity on heat and mass transfers at the surface of a circular cylinder and an elliptical cylinder, axis ratio 4, Int. J. Heat Mass Transfer 38 (1995) 1735–1749.
[2] A. Kondjoyan, J.D. Daudin, Heat and mass transfer coefficients at the surface of a pork hindquarter, J. Food Eng. 32 (1996) 225–240.
[3] L. Ghisalberti, A. Kondjoyan, Convective heat transfer coefficients between air flow and a short cylinder, effect of air velocity and turbulence, effect of body shape dimensions and position in the flow, J. Food Eng. 42 (1999) 33–44.
[4] T. Igarashi, Local heat transfer from a square prism to an airstream, Int. J. Heat Mass Transfer 29 (1986) 777–784.
[5] V. Natarajan, M.K. Chyu, Effect of flow angle-of-attack on the local heat/mass transfer from a wall-mounted cube, J. Heat Transfer 116 (1994) 552–560.
[6] E.M. Sparrow, F. Samie, Measured heat transfer coefficients at an adjacent to the tip of a wall-attached cylinder in cross-flow – application to fins, J. Heat Transfer 103 (1981) 778–784.
[7] A. Slaouti, J.H. Gerrard, An experimental investigation on the end effects on the wake of a circular cylinder towed through water at low Reynolds numbers, J. Fluid Mech. 112 (1981) 297–314.
[8] S. Tanaka, S. Murata, An investigation of the wake structure and aerodynamic characteristics of a finite circular cylinder (time-averaged wake structures behind circular cylinders with various aspect ratios), JSME Int. J. Ser. B, Fluids Therm. Eng. 42 (1999) 178–187.
[9] D.J. Farivar, Turbulent uniform flow around cylinders of finite length, AIAA J. (1981) 275–280.
[10] R.I. Basu, Aerodynamic forces on structures of circular cross-section, Part 2. The influence of turbulence and three-dimensional effects, J. Wind Eng. 24 (1986) 33–59.

[11] L. Ghisalberti, A. Kondjoyan, A method to map out the local transfer coefficient on the complete surface of a circular cylinder subjected to an air flow, Int. J. Therm. Sci. 40 (2001) 738–752.

[12] J.D. Daudin, A. Kondjoyan, Influence de l'indice de turbulence de l'écoulement sur les procédés de traitement thermique de solides par l'air, Lavoisier. Récents Progrès En Génie Des Procédés 5 (1991) 287–293.